AIMS Energy, 13(5): 1195–1218.
DOI: 10.3934/energy.2025044
Received: 15 May 2025
Revised: 19 July 2025
Accepted: 15 August 2025
Published: 24 September 2025

https://www.aimspress.com/journal/energy

Research article

Adaptive neuro-fuzzy control for dual boost converter in fuel cell electric vehicles

Panimathi B[1], K. Deepa[1,*], S.V. Tresa Sangeetha[2], Porselvi T[3] and Mohan Lal Kolhe[4]

[1] Department of Electrical and Electronics Engineering, Amrita School of Engineering, Amrita Vishwa Vidyapeetham, Choodasandra, Bengaluru 560035, Karnataka, India
[2] Engineering Department, Electrical and Electronics Section, University of Technology and Applied Science - Al Mussanah, Oman
[3] Department of Electrical and Electronics Engineering, Sri Sairam Engineering College, Sai Leo Nagar, Chennai, India
[4] Faculty of Engineering and Science, University of Agder, 4604 Kristiansand, Norway

* **Correspondence:** Email: k_deepa@bl.amrita.edu; Tel: +919980005171.

Abstract: Electric vehicles powered by fuel cells provide clean energy with zero emissions and are highly sustainable. Increased demand for sustainable transport has rendered hydrogen fuel cell electric vehicles (FCEVs) a feasible choice compared to conventional internal combustion engines. However, efficiency is significantly dependent on the strength of power electronic interfaces and smart control. This research combined an adaptive neuro fuzzy inference system (ANFIS) with two switched boost-converters to manage power from a fuel cell to a battery to deliver a constant voltage and to achieve optimal energy use. This improved the voltage regulation capability, particularly during load change. ANFIS combines the learning ability of neural networks with the decision structure of fuzzy logic. The hybrid approach is conducive to faster response, greater flexibility, and better energy efficiency over varying operating conditions. The ANFIS model recorded a value of root mean square error (RMSE) of 0.0024, confirming high accuracy in dynamic loading handling. Simulation outcomes support the effectiveness of the system and better performance when compared with traditional proportional integral (PI) controllers.

Keywords: neuro fuzzy inference system; hydrogen fuel cell; dual-switch interleaved boost converter; dynamic load control; energy management; power flow optimization; voltage regulation and clean energy

1. Introduction

Electric vehicles (EVs) are revolutionizing sustainable transportation, with zero-emission potential if powered by renewable energy. An efficient power management through intelligent control and advanced converters ensures optimal charging and performance of EVs, thereby enhancing the reliability and longevity of EVs. Progress has been made in hydrogen production, storage, and refueling in terms of costs, efficiency, and emissions, offering electrolysis as a sustainable alternative, as well as innovations in storage and refueling for transport decarbonization. Hydrogen fuel cell vehicles [1] pose leakage, fire, and explosion risks, requiring strict monitoring and regulation. Hydrogen sensors have been discussed as integrated and safe in transportation. An optimized voltage gain in photovoltaic systems [2] under conditions of varying operation is critical for the efficient distribution of renewable energy. It uses a Zeta converter [3] with maximum power point tracking using ANFIS and grey wolf optimization (GWO) toward enhanced power conversion and efficiency for electric vehicles. Hybrid electric vehicles (HEVs) with V2X topology [4] and smart energy management system (SEMS) show optimized energy efficiency, minimized emissions, and facilitated grid integration. They optimize power exchange between the battery, engine, and grid for a maximum utilization of renewable energy. A machine learning model [5] has been developed to forecast average charging time for optimizing charging station locations and grid demand management. Dimension reduction and support vector machine yield the best forecasts, allowing efficient energy planning for the expanding EV sector.

1.1. Motivation

The inspiration for this research comes from the need for cleaner and more efficient energy management technologies in the transportation industry, urged by increasing concerns regarding climate change, urban air pollution, and depleting fossil fuels. Hydrogen fuel cells are a promising zero-emission energy carrier for EVs, with high energy efficiency and being environmentally sustainable. Nevertheless, fuel cells are nonlinear by nature and have slow dynamic response; thus, their direct integration would be inappropriate in the absence of an intelligent control interface. Under highly dynamic load conditions, this can lead to voltage instability, poor power regulation efficiency, and poor battery charging performance. To overcome these challenges, this study suggests a control scheme using ANFIS with an integrated dual-switch interleaved boost converter. This architecture of the converter not only enhances voltage gain and minimizes current ripple suppression but also improves power transfer efficiency from the fuel cell to the lithium-ion battery. The ANFIS controller, which is trained from PI-based simulation data, dynamically controls the operation of the converter and is simulated under both static and dynamic load conditions; it shows better performance and adaptability than traditional control schemes. Simulation outputs in MATLAB/Simulink validate that the ANFIS-controlled system provides quicker dynamic response, enhanced voltage stability, and enhanced overall efficiency without compromising compatibility for future hardware implementation and commercial rollout in sustainable EV platforms.

1.2. Related works

This section reviews recent contributions focused on sustainable infrastructure, advanced DC-DC converter designs, and adaptive control algorithms for enhanced charging performance. A survey comparison analysis with the proposed work is given in Table 1. The suggested design [6] optimizes EV infrastructure by proposing routes and charging stations using the first-come, first-served (FCFS) algorithm with state of charge (SoC). A comparison between ant colony optimization (ACO) and Dijkstra algorithms indicates that ACO is more suitable for shortest path planning. The areas of future research involve the integration of real-time traffic data as well as machine learning in the estimation of the trip distance. This work uses sensor data and ML models to forecast SoC and state of health (SOH) for proactive battery maintenance. The long short-term memory-support vector regression (LSTM-SVR) hybrid model [7] was found to be most effective, improving battery performance and avoiding possible failures.

Increasing unmanned aerial vehicle (UAV) flight duration is important, as it relies on battery capacity and efficiency. ML models are used to reliably predict the SoC for lithium-polymer and lithium-ion batteries. The SVR was found to be most precise, and lithium-polymer batteries were determined to be the best option for UAV use [8]. The battery management system (BMS) elaborates on advanced BMS techniques and challenges related to the adoption of EVs, regarding charge-discharge control, thermal management, and SoC estimation [9]. A previous work evaluated the optimization of PV-based electric bus battery swapping stations using metaheuristic techniques [10], namely binary bat algorithm (BBA), wolf optimization algorithm (WOA), and GWO, to reduce energy costs by 27.63% and peak demand by 23.43%. A novel SC stage was proposed in [11] for a three-phase switched-capacitor boost multilevel inverter (TSCBI) with inherent voltage balancing and improved efficiency for solar and electric vehicle applications. A power factor-corrected Y-cell modified boost (YCMB) converter-fed EV charger [12] with total harmonic distortion (THD) resulted in up to 95% efficiency. MATLAB simulations and experiments are presented to validate the improved performance of the proposed system for low-to-medium power applications.

As the transport sector is significantly calling for electrification to reduce pollution, an improved power factor correction (PFC) topology [13] for the EV chargers has ensured 2.53% THD and provides efficient standard-compliant charging. A comparison between two-phase and three-phase interleaved DC-DC converters with parallel MOSFETs has been conducted in [14], discussing the tradeoffs involved in cost, voltage regulation, and current balancing. A new interleaved PWM (IPWM) technique was proposed to maximize efficiency and current distribution under SoC conditions. The adaptive PID LFC with ANN and ANFIS was trained on GA-optimized parameters [15], thereby ensuring that optimal performance is maintained under changing load conditions. A comparative analysis showed that ANFIS outperforms error metrics such as IAE, ITAE, and ISE. The ANFIS-based fractional-order PID controller optimized with ACO for EV speed control was presented in [16], ensuring high accuracy and robustness. The controller was tested using a new European driving cycle (NEDC) and outperformed the traditional fuzzy-based controllers with a low RMSE. The ANFIS-controlled boost and bidirectional buck-boost converter [17] improved voltage stability and performance over PI and FLC controllers.

Table 1. Comparative analysis.

Paper No	Topology	Control strategies	Application scenario
Proposed work	Dual-switch interleaved boost converter: offers higher voltage gain, lower current ripple, faster dynamic response; the use of two out-of-phase switches reduces stress on passive components and improves control flexibility, making it ideal for onboard EV systems.	ANFIS (trained with PI data using Gaussian membership functions and hybrid learning)	Hydrogen fuel cell-based onboard EV charging system under static and dynamic load conditions
[17]	Basic boost, bidirectional buck-boost, dual-stage operation with moderate boost capability: more suitable for steady-state microgrid integration but has higher ripple, lower voltage lift, and less efficiency under variable EV charging loads.	ANFIS compared with PI and FLC for SoC and load regulation	DC microgrid system integrating PV, fuel cell, and BESS
[18]	Switched capacitor Z-source converter (SCZSC): voltage gain achieved through passive capacitor switching. Offers modularity but has higher electromagnetic interference (EMI), slower dynamic behavior, and limited scalability for onboard use.	MIMO–ANFIS controller with optimized fuzzy rules	Solar-fuel cell hybrid off-board EV charging

Dual-boost converter was presented to reduce switching losses and enhance efficiency in high-frequency applications [19]. The circuit facilitates soft-switching at turn-on and turn-off, thereby improving overall converter performance. In addition, to minimize the input current ripple and enhance power quality for renewable energy applications [20]. The EV charging stations focus on the integration of intelligent energy infrastructure with power electronics that are optimized for efficiency. The developed solar-powered electric vehicle charging station in [21] with IoT-based monitoring and user authentication through radio frequency identification (RFID) was tested for techno-economic viability with MPPT control and cloud interface. An ultra-fast charging through a dual active bridge (DAB) converter [22], tested with model predictive control (MPC) and fuzzy logic, drastically enhanced transient performance compared to phase-shift modulation (PSM) in simulations. Regarding green infrastructure, an adaptive control-based isolated bidirectional converter for grid-to-vehicle (G2V) and vehicle-to-grid (V2G) charging was explored [23], which incorporates renewable energy sources for the efficient flow of power. The system revealed improved stability and energy transfer capability under dynamic grid and load conditions with smart converter control strategies. In ANFIS-based parameter estimation [24] was used in a two-phase interleaved dual-cascaded boost converter to allow adaptive voltage regulation with reliable converter performance. Moreover, reference [25] suggested a smart control system based on ANFIS for a grid-connected hybrid renewable energy system with PV and wind power. The controller aimed to improve power flow and voltage stability with changing weather conditions.

Using renewable energy is critical to achieving world zero-emission goals in transportation electrification. Hybrid renewable energy systems (HRES), comprising solar PV, wind, and energy storage, have been extensively studied for their ability to efficiently and sustainably power stationary infrastructure such as railway systems [26]. At the level of road transport, a detailed review [27] examined the transition to greener options by assessing the technical, infrastructural, and regulatory hurdles in deploying electric vehicles on a large scale. Public transit, especially electrified bus systems,

has also emerged as an area of strategic concern for urban decarbonization. Reference [28] investigated the optimization of fleet operation, energy supply planning, and cost-benefit analysis under electrification scenarios. Additionally, the synergy between electric vehicles and renewable energy technologies [29] has been underscored in simulation-based research, indicating that integrating EVs with renewables not only maximizes energy use but also facilitates grid flexibility and decarbonization initiatives.

1.3. Major contributions

The major contributions of this research are as follows:

i. It highlights a zero-emission onboard charging system for hydrogen-powered electric vehicles by integrating a hydrogen fuel cell for a dual switch boost converter with ANFIS-based controlled strategy. The proposed system includes balanced battery units that independently demonstrate charging and discharging modes, closely resembling real-time operation.
ii. It achieves superior voltage stability and reduced charging losses compared to standard single switch architectures, efficient power regulation of a fuel cell, and charging a lithium-ion battery in constant current–constant voltage mode. The fuel cell serving as the primary energy source operates with the regulated supply of hydrogen fuel and air, enabling flexibility and adaptive power generation under varying vehicle demands.
iii. The ANFIS closed-loop control outperforms conventional strategies and is further examined under static and dynamic load variations to prevent open-loop instabilities. A detailed analysis of converter stability, time over epochs evaluation, rate of change in SOC, and time response characteristics of controllers is carried out to ensure robust operation.

With respect to its potential, the above framework can be expanded to hybrid vehicle systems where the energy has to be dynamically controlled between multiple sources (fuel cell, battery, supercapacitor), to regenerative braking energy recovery through control of the converter enabling bidirectional flow, and renewable energy-based charging stations, wherein the fluctuating output can be controlled in accordance with the same adaptive control principles. Overall, this work presents sustainable, intelligent, and adaptive powertrains and offers a flexible and scalable solution for future clean mobility platforms.

1.4. Paper organization

The work follows a coherent flow where the system description part starts with defining the overall system block diagram, fuel cell operations, dual boost converter stability, and control strategy, followed by mathematical equations and battery specifications. The simulation and results part subsequently validates system operation under dynamic modes, demonstrating stability and improved power transfer in Section 3. Finally, the conclusion in Section 4 synthesizes major findings and discusses broader implications of the proposed approach to fuel cell-based EV drives.

2. System description

2.1. Block diagram

The proposed block diagram (Figure 1) represents an ANFIS-controlled dual boost converter for the energy management system on a fuel cell-powered EV. The power obtained from hydrogen and oxygen in a fuel cell stack is fed into the dual boost converter, where the power is regulated. Optimization of the power flow is done through the dynamic adjustment of converter parameters by the ANFIS controller. During charging, the converter transfers power from the fuel cell to the battery. In case of discharging, the battery transfers power to the EV motor. This system ensures efficient energy management, which enhances performance and reliability in EV applications.

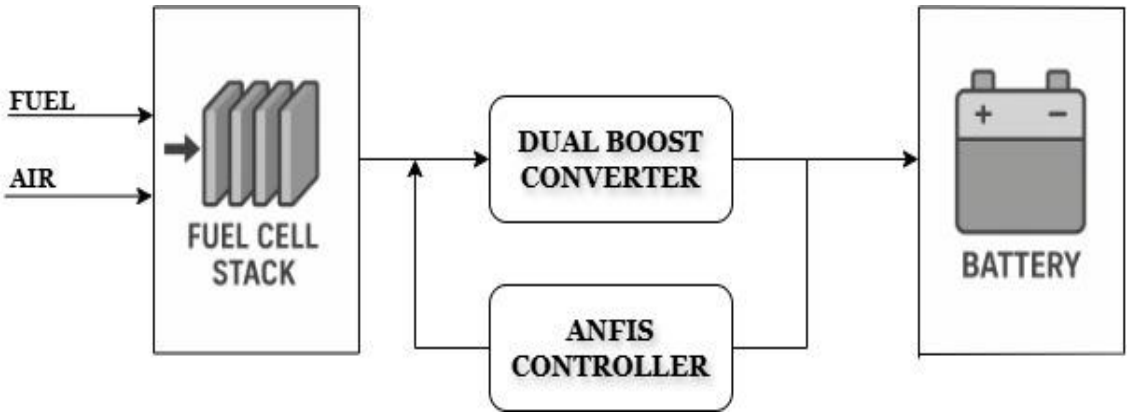

Figure 1. Pictorial representation of overall system.

2.2. Fuel cell architecture

The molar concentration determines the flow rates for fuel (hydrogen) and air (oxygen) that are used for the electrochemical reaction in the fuel cell, where it is converted into electricity, water, and heat, providing a clean and efficient energy source. Equation (1) represents the molar flow rate $\dot{n}$ that includes the universal gas constant R, temperature T, pressure P, Faraday's constant F, the stoichiometric ratio, and efficiency factors that control the reactant availability. In addition, Q is the heat energy, u (1) represents the control input variable used to vary fuel and air flow, V refers to the voltage, and 60,000 is a scaling factor for unit conversion. A right balance of fuel and oxidant prevents losses in efficiency while maximizing the energy conversion through this equation.

$$\dot{n} = \frac{60000 \times R \times (T_{\text{operating}}) \times Q \times u(1)}{n \times F \times P \times V} \tag{1}$$

The selected power source is a proton exchange membrane fuel cell (PEMFC) that will be used to supply power during operation to the EV battery. Each stack supplies 6.4 kW for the simulated fuel cell; the nominal stack power is 5.9985 kW, and the peak power output is 8.325 kW, with an output terminal resistance of 78.33 mΩ per cell. In Table 2, the electrical and input specifications of the fuel-cell stack are summarized.

Table 2. Fuel cell specifications.

Parameters	Values
Stack voltage	45 V
Operating current	133 A
Maximum current	255 A at 37 V
Number of cells used	65
Operating temperature	65 ℃
Fuel flow rate	300 lpm
H_2 and O_2 utilization	99.56% and 23.6%
Exchange coefficient	0.60645

Figure 2 illustrates the voltage-current and power-current characteristics of the designed PEMFC. At 225 A and 37 V, the fuel cell is set at its operating point to find a maximum power output of 8.325 kW. It thus presents peak performance. On the other hand, at 133 A and 45 V, the module works at its nominal power of 6 kW, which provides stable and efficient energy delivery. These features add up to a reliable and adaptable fuel cell for operations in electric vehicle systems for extended periods.

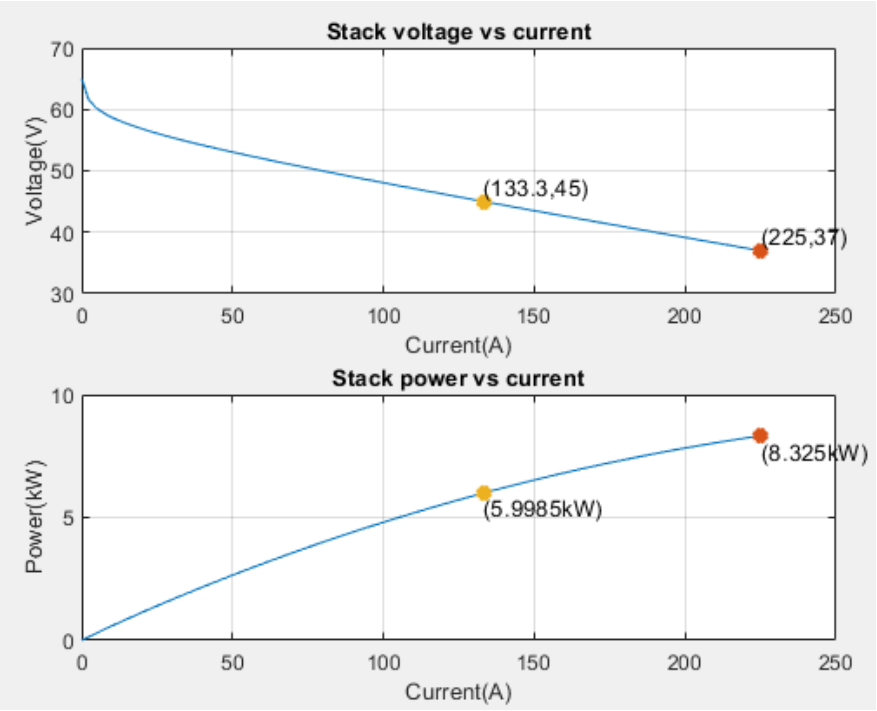

Figure 2. Stack voltage vs. current and power vs. current.

The parametric values of the FC stack show a flow rate of about 19.9 L/min. The oxygen and hydrogen utilization rates are 23.6% and 99.56%, respectively. The air and fuel consumption of the stack are 70.9 L/min and 19.8 L/min, respectively. As shown in Figure 3, the FC stack has an efficiency of about 69.5%.

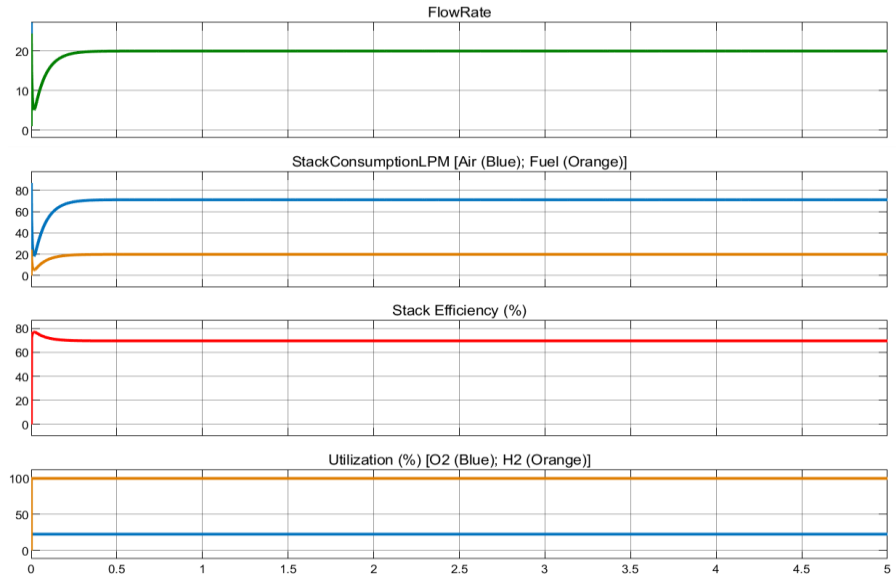

Figure 3. FC stack parameters.

2.3. Interleaved converter

The proposed dual boost converter in [19] is integrated for voltage boosting, providing efficient power to flow into the battery with enhancement of the voltage output from the fuel cell. The two interleaved inductors are incorporated in Figure 4a, with their diodes D_1 and D_2, a capacitor C, and the switches SW_1 and SW_2. The switches switch between ON and OFF states during operation, which in turn enables energy storage and then release by the inductors, thereby causing a boost in voltage. This also enables a smooth power transfer. In such control, PWM pulses are applied for the modulation of the output voltage to optimize efficiency with varying load conditions. Again, the capacitor provides stabilization in the output voltage, ensuring effective charging and power discharge.

State 1:

The equivalent circuit is examined using KVL as follows, considering the switching states as SW1 = 1 and SW2 = 0:

L3 ensures equal current distribution between the inductors, as shown in Figure 4d. It smooths out the transition between the two switching states and prevents large inrush currents.

In Figure 4b, L1 is charging from V1, and L2 is discharging to the load through D2 and L3. When both switches toggle states, L3 releases its stored energy to the inductor that has a lower current. The current through the inductors are given by Eqs (2)–(4).

$$\frac{dI_{L1}}{dt} = \frac{V_1}{L1} \tag{2}$$

$$\frac{dI_{L2}}{dt} = \frac{V_1 - V_R}{L2} \tag{3}$$

$$\frac{dI_{L3}}{dt} = \frac{V_R}{L3} \tag{4}$$

State 2:
when SW1 = 0, SW2 = 1, The obtained equations are (5)–(7), where L2 is charging from V1, and L1 is discharging to the load through D1 and L3 (Figure 4c).

$$\frac{dI_{L1}}{dt} = \frac{V_1 - V_R}{L1} \tag{5}$$

$$\frac{dI_{L2}}{dt} = \frac{V_1}{L2} \tag{6}$$

$$\frac{dI_{L3}}{dt} = \frac{V_R}{L3} \tag{7}$$

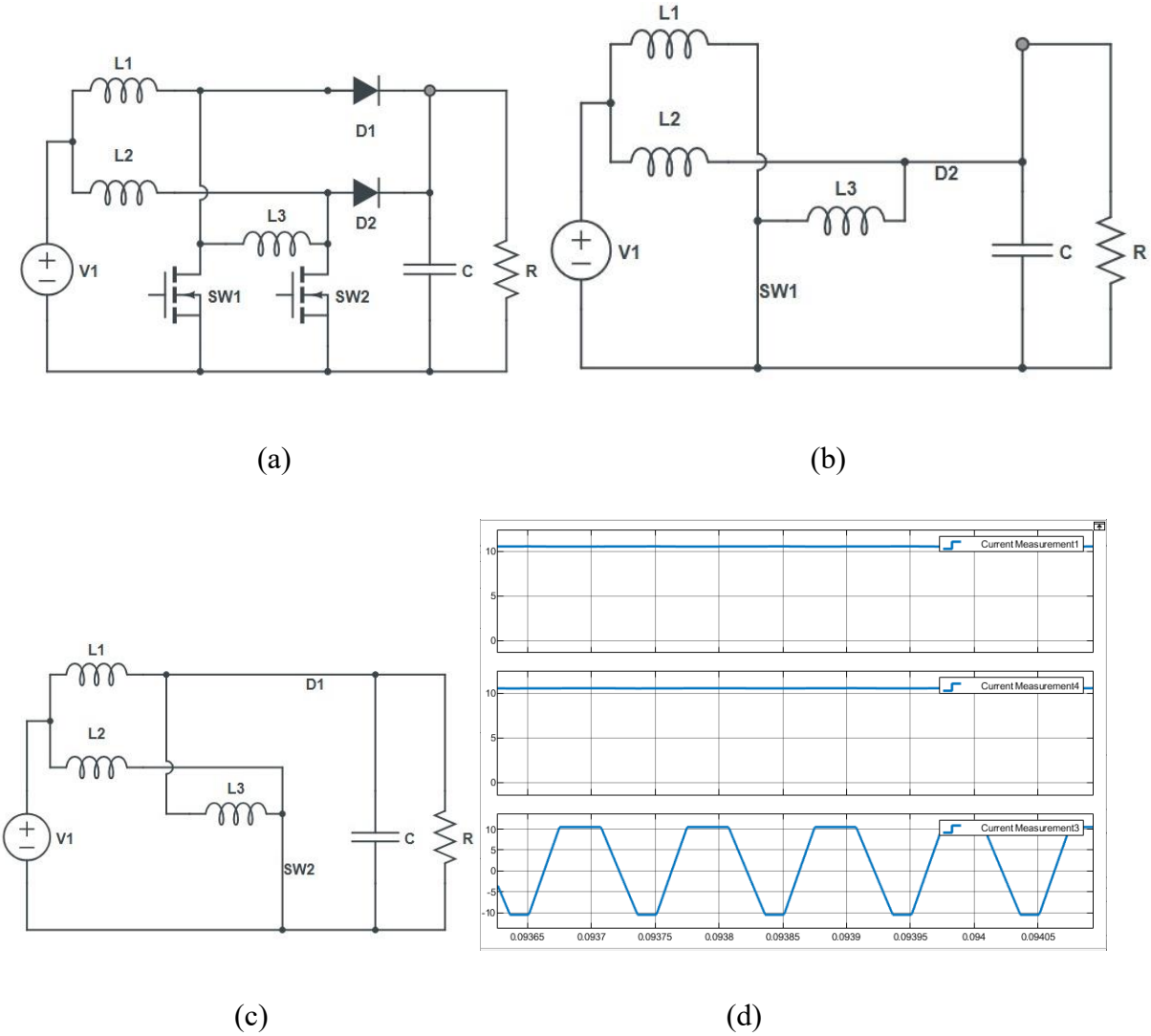

Figure 4. (a) Dual boost converter; (b) Interleaved converter_state1; (c) Interleaved converter_state2; (d) Inductor current profiles.

The terms S1 and S2 are the switching states of SW1 and SW2 in the capacitor voltage Eq (8) in the converter. The ideal voltage-gain in Eq (9) for two-phase interleaved boost converter is as follows:

$$\frac{dV_C}{dt} = \frac{(1-S_1)\, I_{L1} + (1-S_2)\, I_{L2} - \frac{V_R}{R}}{C} \tag{8}$$

$$G = \frac{V_R}{V_1} = \frac{1}{1-D/2} \tag{9}$$

The voltage transfer function using Laplace transform from [20] is used to analyze the system stability,

$$\frac{U_o(s)}{U_i(s)} = \frac{1}{L_{eq}Cs^2 + \frac{L_{eq}}{R}s + (1-D)^2} \tag{10}$$

where D is the duty cycle of each switch.

The system stability is examined through step response, Bode plot, and root locus by adopting a derived transfer function in Eq (10) for this interleaved converter from [20]. The step response in Figure 5 has a rise time of 169 seconds and a settling time of 301 seconds, with no oscillations in the transient period, and with a peak deviation of 1. The Bode plot in Figure 6 provides a gain margin (GM) of 83.8 dB at 55.3 rad/s and a phase margin (PM) of 90° at 0.013 rad/s, both of which are positive, thus assuring stability. The root locus plot in Figure 7 shows that all poles are in the left-half plane, further confirming system stability. The GM greater than 10 implies that the converter can withstand variations in converter parameters, load, and disturbances. A phase margin (PM) greater than 60 makes the response slow, resulting in an overdamped system.

The performance is improved further by substituting the traditional PI controller with an ANFIS, which can considerably improve response speed by minimizing rise and settling time, as validated by result analysis.

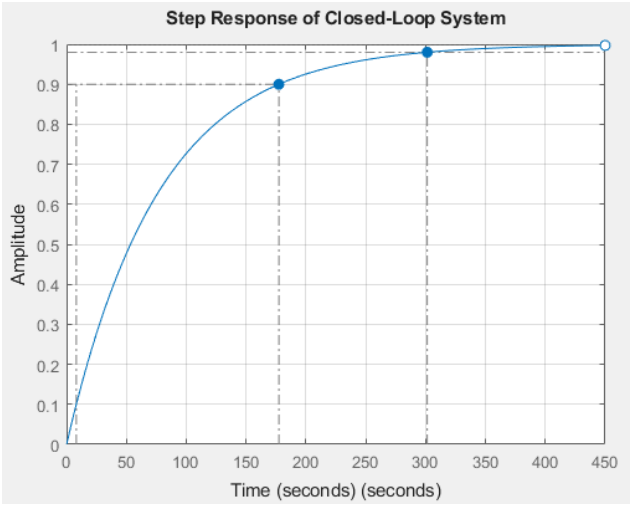

Figure 5. The step response of the closed-loop system.

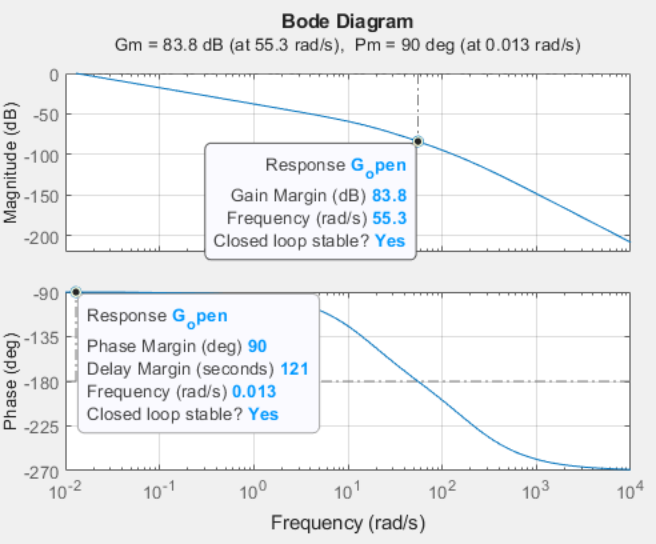

Figure 6. Bode plot for the interleaved converter.

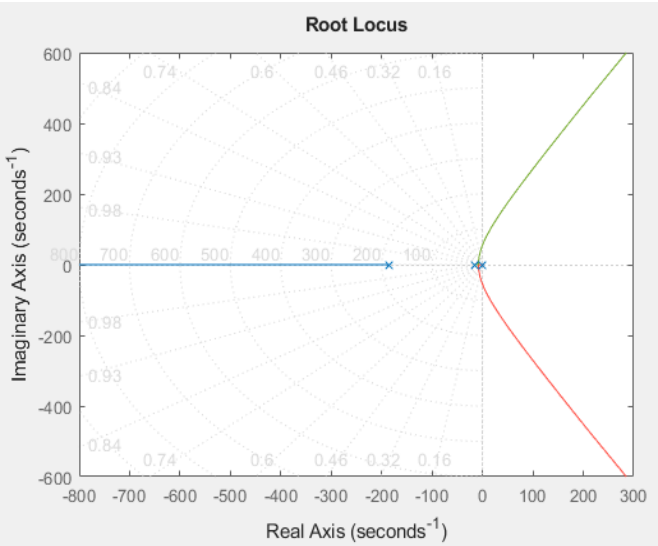

Figure 7. Root locus for the interleaved converter.

2.4. ANFIS controller

The ANFIS (adaptive neuro-fuzzy inference system) controller in Figure 8 combines fuzzy logic and neural networks for converter operation control. This may consist of multiple layers, such as fuzzification, rule evaluation, normalization, defuzzification, and summation for output. The controller applies linear Gaussian membership functions in Figure 9 to map the input variables and process them according to a structured rule-based approach. The system, through training, alters the nodes and interconnections to optimize decision-making based on the variations in voltage and load. Through learning from the input-output relationship, ANFIS dynamically tunes its control strategy while being quite precise in the regulation of the converter and enhancing its overall performance for electric

vehicle charging and discharging applications.

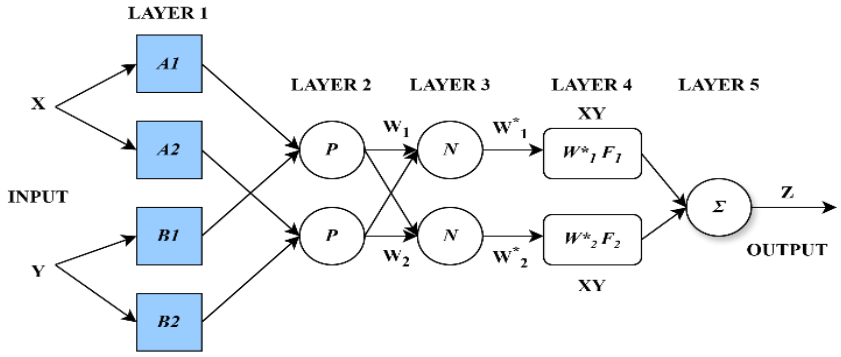

Figure 8. Structure of ANFIS.

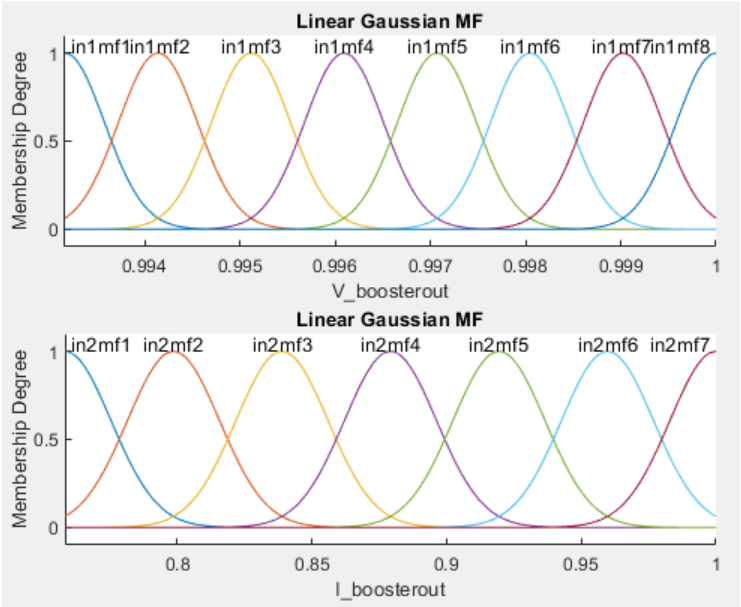

Figure 9. Gaussian MF.

Each rule in the fuzzy system in Eq (11) is based on input fuzzy sets A_i as a and B_i as b. m_i, n_i, c_i are learning parameters adjusted via hybrid learning, and the duty cycle is calculated as the weighted sum of rule outputs.

$$Z_1 = m_1 a + n_1 b + c_1; Z_2 = m_2 a + n_2 b + c_2 \tag{11}$$

An example of rules generated in the process is listed below:

Rule 1: If Vout is low and I_out is high, then Duty = $m_1 \cdot V + n_1 \cdot I + c_1$

Rule 2: When Vout is high and I_out is low, then Duty = $m_2 \cdot V + n_2 \cdot I + c_2$

The final output z is obtained using Eq (12) by computing the weighted sum of the rule outputs, where w_i is firing strength of fuzzy rules.

$$z = \frac{w_1}{w_1+w_2} Z_1 + \frac{w_2}{w_1+w_2} Z_2 \quad (12)$$

Thus, the final Eq (13) represents the output of a Sugeno-based fuzzy inference system, where w_i^* is the normalized output weight of layer 3.

$$z = (w_1^* a)m_1 + (w_1^* b)n_1 + w_1^* c_1 + (w_2^* a)m_2 + (w_2^* b)n_2 + w_2^* c_2 \quad (13)$$

Algorithm: Pseudo-code for the controller implementation:

1. Formulate the closed-loop PI-based control for interleaved dual switch boost converter.
2. At every time step of the simulation *t*:
   a. Get the V_out(t) and I_out(t) of the converter as tuples.
   b. Determine the output duty cycle D_PI(t).
3. Exit the loop after the dataset is created in the workspace.
4. Pre-process the dataset by outlier removal, normalization, and train-test split.
5. Initialize the ANFIS model with FIS employing grid partitioning to auto-generate rules.
6. Use the Gaussian membership functions (MFs) for each input variable.
7. Train the ANFIS model using the following:
   a. Input variables: V_out, I_out and Target variable: D_PI.
   b. Adjust the hybrid learning optimization technique (backpropagation and least squares).
   d. Fix the training parameters like epochs and error tolerance.
8. Test the trained ANFIS model through error metrics and plot across train, test, and check datasets.
9. Save the trained ANFIS model for control deployment.
10. Begin real-time simulation or hardware-in-the-loop run.
11. During the execution:
    a. Log V_out and I_out in real-time.
    b. Scale input values and predict the optimal duty cycle.
    c. Generate PWM signals and control switches S1 and S2 correspondingly.
    d. Check the battery State of Charge (SOC) and sustain the constant current-constant voltage (CC-CV) profile.
12. End the real-time loop.

2.5. Battery

The proposed lithium-ion battery in Table 3 has an assigned capacity rating of 70 Ah and an initial SOC of 60%. Thus, it supports charging from battery 1 of nominal voltage 180 V and discharging from battery 2 with a constant nominal voltage level of 220 V.

Table 3. Battery specifications.

Parameters	Charging	Discharging
Nominal voltage	180	220
Rated capacity	70	70
Initial SOC (%)	60	60
Battery response time (sec.)	0.5	0.5

3. Simulation and results

The integrated system in Figure 10a involves a dual switch booster configuration [19] in combination with the fuel cell and battery in control. The performance of the fuel cell is sensitive to the management of the flow of hydrogen and oxygen, as indicated by the molar flow of Eq (1).

First, the system was tested with an open-loop condition, where the input power was managed without any feedback control. The performance in Figure 11 was assessed using reliable gate pulses under static load conditions of 3355 W and 224 V, which settles at 0.6 s, establishing a baseline against understanding the system's behavior with fuel cell dynamics.

For the static closed-loop operation in Figure 12, the control strategy was improved by applying a proportional-integral controller (P = 0.0005, I = 0.015). This PI controller was chosen since it is less complicated, well-proven in combining steady-state errors, and stabilizes at 0.4 s to ensure that the output voltage falls within 225 V, while the input voltage is 65 V and power is within 3408 W.

When the system faces dynamic load variations, several challenges emerge in maintaining system stability and efficiency. At rapid load transients where the system could not respond fast enough to sudden demand, there is an increased need for a greater control mechanism (Figure 10b) to dynamically regulate the power flow while maintaining stable voltages.

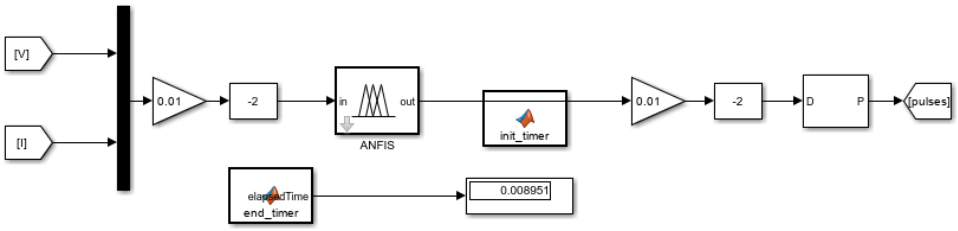

(a)

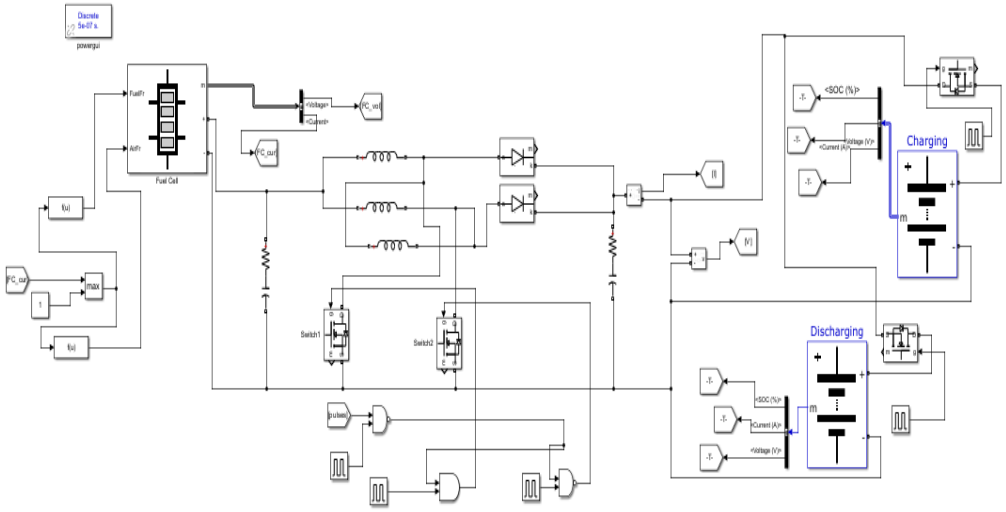

(b)

Figure 10. (a) Schematic diagram of ANFIS controller; (b) The overall proposed system for a hybrid electric powertrain.

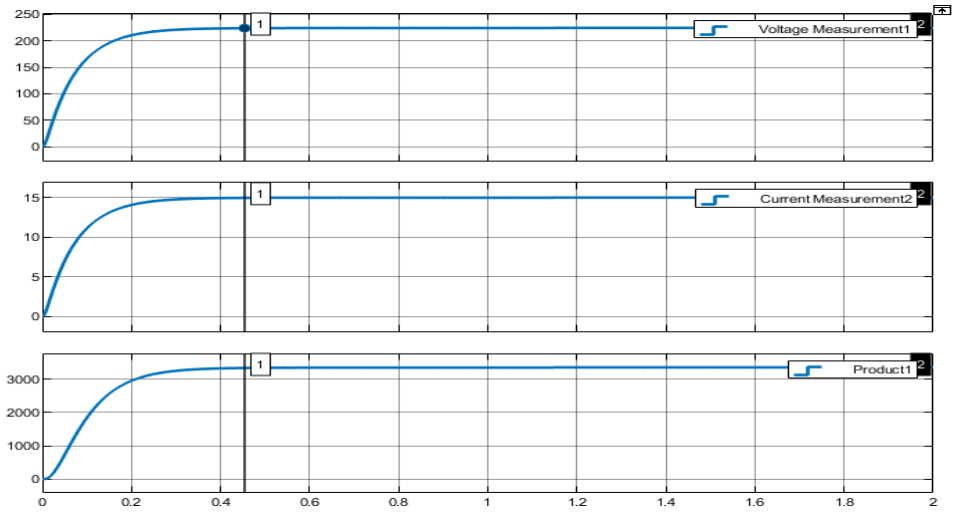

Figure 11. Open-loop output with a rated load.

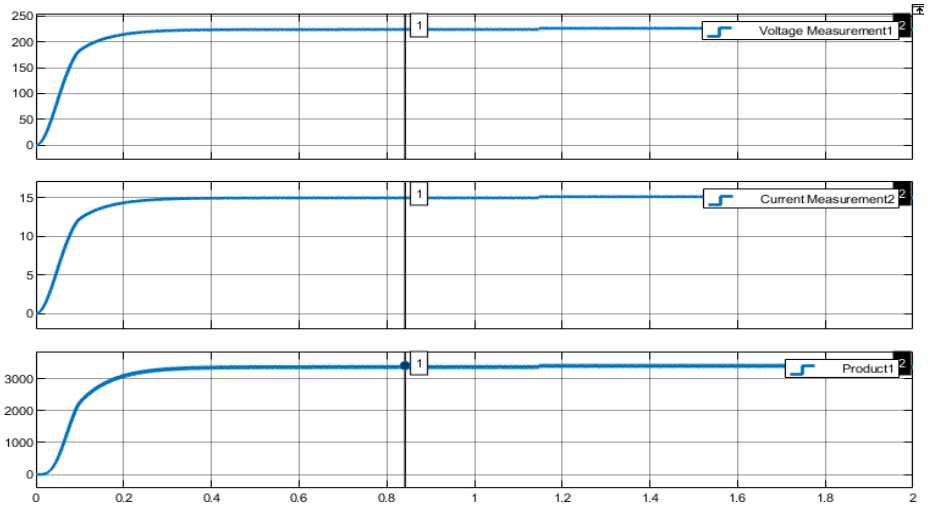

Figure 12. Closed-loop output with PI controller.

To test and optimize the system's response, Simulink was used. This method ensured that there was no need for historical data, which were supposed to exist before running the control system. The data in Figure 13 has 101,005 rows and 3 columns, which include booster voltage, current, and duty cycle during PI closed-loop analysis under dynamic load changes, used to train FIS and to understand how the system responded to real-time conditions. Normalizing the data improved the ANFIS model accuracy and enhanced the root mean square error (RMSE) for load prediction and control.

```
>> mat
Original data size: 101005 rows, 3 columns
Data size after outlier removal: 99839 rows, 3 columns
Training data size: 69887 rows
Testing data size: 29952 rows
Data preprocessing completed and saved.
```

Figure 13. Data splitting and preprocessing.

A normalized dataset split at a ratio of 70:30 was utilized for both ANFIS training and testing with a linear Gaussian membership function. Applying grid partitioning for fuzzy inference system with a size of 147 nodes and training over a span of epochs of 50 resulted in Figure 14, with an average minimal error of 0.0024.

```
ANFIS info:
    Number of nodes: 147
    Number of linear parameters: 168
    Number of nonlinear parameters: 30
    Total number of parameters: 198
    Number of training data pairs: 69887
    Number of checking data pairs: 5990
    Number of fuzzy rules: 56
```

Figure 14. ANFIS model summary.

The graphical plots in Figures 15, 16, and 17 of ANFIS training, testing, and checking data were created to further assess the performance of the model.

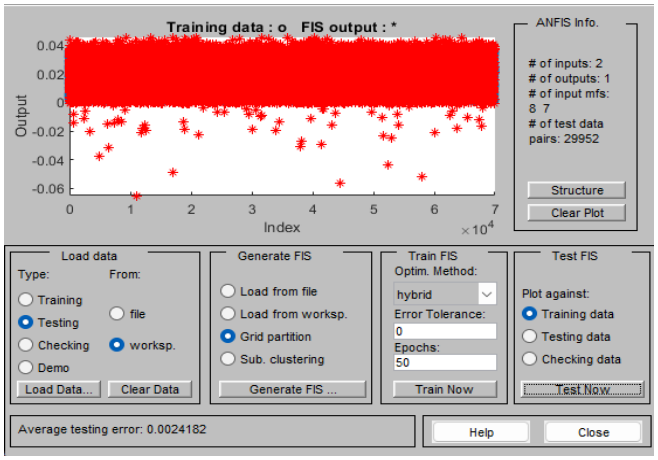

Figure 15. Training data analysis.

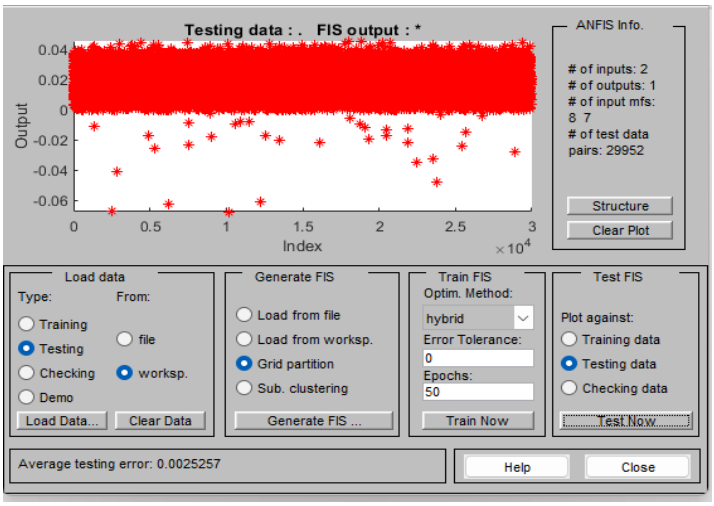

Figure 16. Testing data analysis.

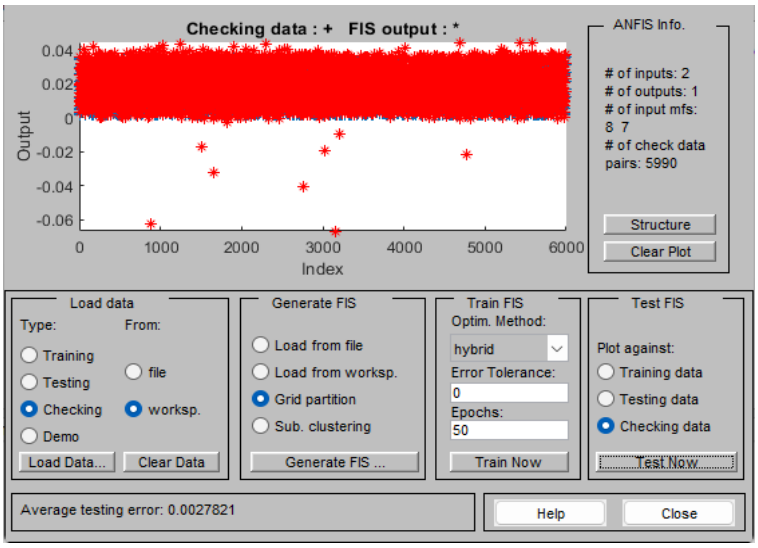

Figure 17. Checking data visualization.

The checking dataset, comprising 20% of the tested set, serves as an independent validation measure to assess the model's generalization capability. The plot in Figure 17 enables a direct comparison between the predicted FIS output and actual data, demonstrating the accuracy and reliability of the trained ANFIS model. The training error plot over 50 epochs shows that there is effective learning and convergence (Figure 18).

The structure of the ANFIS model in Figure 19 was explored with its rule base, membership functions, and node connectivity. The visualization of the train, test, and check plots provides insight into how well the model adapts to datasets, ensuring that it effectively captures the underlying system dynamics. This structural representation enhances understanding of the model's complexity, interpretability, and decision-making process, ensuring both robustness and computational efficiency.

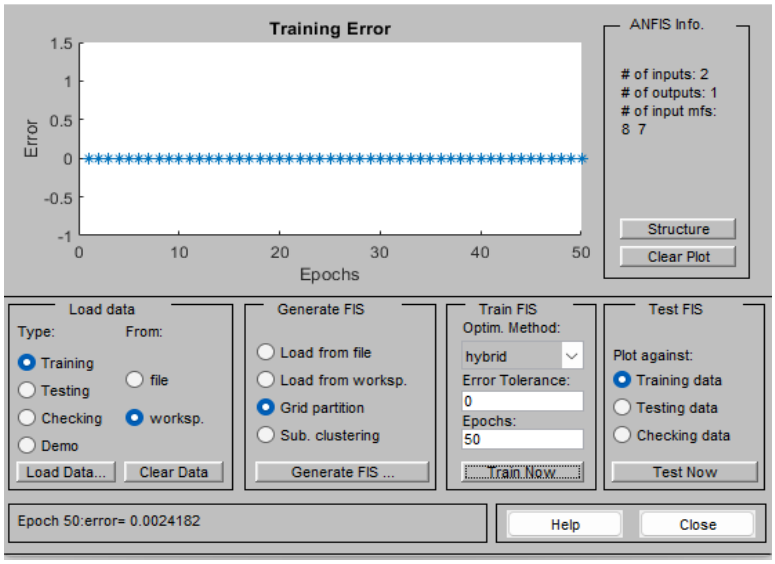

Figure 18. Training RMSE for grid partitioning.

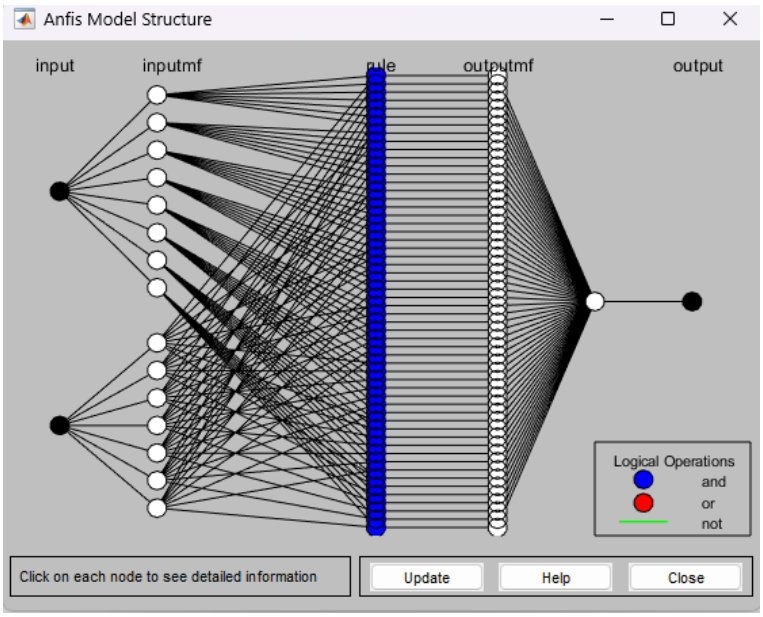

Figure 19. ANFIS architecture for fuzzy rule-based learning.

The trained ANFIS model, instead of PI in the closed system, was replaced along with a gain and bias block using the data in the process to de-normalize the values from the given simulation for the optimal accuracy in predicting dynamic loads to optimize power. The time elapsed indicated in Figure 20 implies that the elapsed time per epoch reduces considerably with increasing epochs. Over 50 epochs took the least time of 0.0012, showing an effective training efficiency (Table 4) and a protective learning curve.

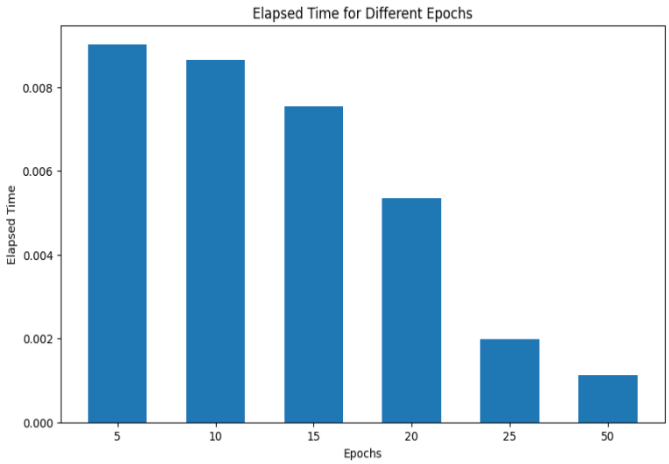

Figure 20. Epochs vs. elapsed time.

Table 4. Evaluation of RMSE and time over epochs.

Epochs	Elapsed time	RMSE
5	0.009	0.004
10	0.0088	0.0035
15	0.0075	0.0030
20	0.0055	0.0028
25	0.002	0.0027
50	0.0012	0.0024

Table 5 shows the analysis for the stopping time of 0.01, showing that the ideal SOC level for stable charging and discharging is between 40% and 60%. As the SOC level rises above this, internal resistance builds up, which decelerates the charge to avoid overcharging and battery degradation. At higher SOC levels during discharging, a faster drop in SOC leads to increased energy loss through heat dissipation with a decrease in the effective power delivered to the motor. Hence, operating within the range of SOC shown in Figure 21 provides balanced performance with reduced energy losses and battery stress that enhances longevity.

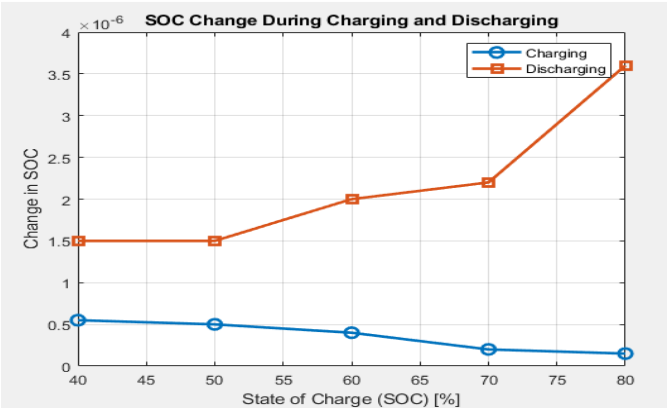

Figure 21. Impact of SOC on battery performance.

Table 5. Rate of change in SOC.

	Change in SOC	
SOC (%)	Charging	Discharging
40	5.5e-7	1.5e-6
50	5e-7	1.5e-6
60	4e-7	2e-6
70	2e-7	2.2e-6
80	1.5e-7	3.6e-6

The ANFIS controller from Table 6 outperforms with 0.0025 s rise time and 0.03 s settling time, which is significantly faster than PI controllers. Under a fuel cell, dual boost battery, fast response is essential for effective energy management and dynamic load regulation. The response is critical for the PI controller under static and dynamic load variations, and this could result in slow power control in the system. Therefore, ANFIS is designed as the optimum controller, which gives the best transient response and stable performance.

Table 6. Time response characteristics of controllers.

Controller	Rising time	Settling time
PI (static load)	0.2	0.5
PI (battery)	0.05	0.15
ANFIS (battery)	0.0025	0.03

The performance of the ANFIS system was given for two parallel battery configurations, as seen in charging and discharging cycles in Figures 22 and 23, which allows the output response to settle at less than 0.03 s. This ensured fast response and efficient energy distribution as the batteries utilize the nominal rated power of the fuel cell. This method effectively balanced the load while achieving a maximum output power of 5985 W, reducing losses and boosting the overall energy efficiency of the system.

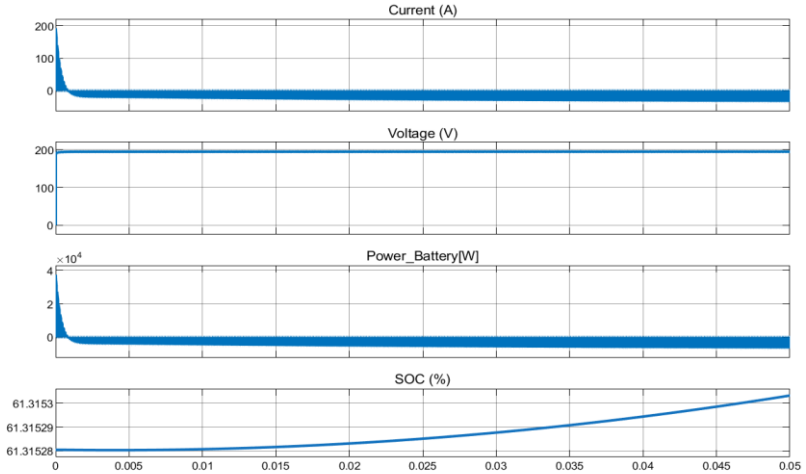

Figure 22. Performance of the battery in charging mode.

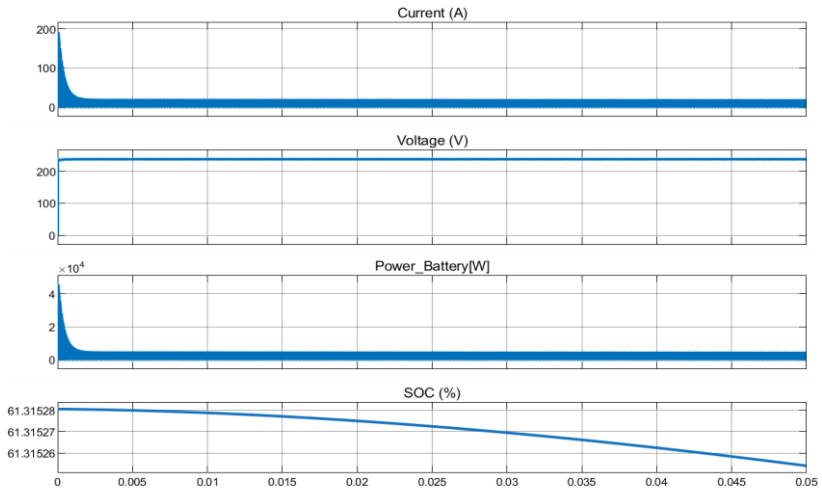

Figure 23. Performance of the battery in discharging mode.

4. Conclusions

This study introduced an ANFIS-adaptive control method for a dual-switch interleaved boost converter in an FCEV charging system based on hydrogen fuel cells. The converter topology provided better voltage gain, lower ripple, and better transient response than traditional single-switch configurations. The ANFIS controller with Gaussian membership functions exhibited better accuracy at an RMSE of 0.0024 and was shown to be robust to regulation under static and dynamic load changes. Simulation findings confirmed the superiority of the proposed system over traditional techniques such as PI and fuzzy control, particularly regarding voltage stability, response time, and energy consumption.

Although the proposed system presents good performance, it is presently assumed to operate at constant ambient conditions. Variations in temperature could drastically affect the efficiency of fuel cells and the dynamics of the system. This shortcoming has now been evidently recognized, and further work shall investigate temperature-aware models and adaptive thermal management techniques. Moreover, current studies [30] validate the incorporation of supercapacitors to boost peak power handling while alleviating stress on battery packs. Thus, our future horizon includes real-time hardware implementation, integration of the battery pack with supercapacitors, and investigation of the use of model predictive control (MPC) to further optimize system operation under multi-variable constraints. The practicality of this design for extended-scale electric mobility use, including V2G and hybrid sources, will also be studied.

Use of AI tools declaration

The authors declare that Artificial Intelligence (AI) tools were not used in the creation of this article.

Acknowledgments

The authors would like to express their gratitude to Amrita Vishwa Vidyapeetham for its support in facilitating this work. This research is funded by the AMRITA Seed Grant; Proposal ID: ASG2022075, Amrita Vishwa Vidyapeetham, India; proposal title: Autonomous E-Mobility Centre.

Conflict of interest

All authors declare that there are no competing interests. Mohan Lal Kolhe is a Guest Editor for AIMS Energy and was not involved in the editorial review or the decision to publish this article. All authors declare that there are no competing interests.

Author contributions

System Description, P. B. and K. D.; Simulation and Result Analysis, P. B. and K. D.; Draft Preparation, P. B.; Writing Review and Editing, P. B. and K. D.; Supervision, K. D., S.V., P.T., M.K.; Project Administration, K. D., S.V., P.T., M.K.; All authors reviewed the manuscript.

References

1. Halder P, Babaie M, Salek F, et al. (2023) Advancements in hydrogen production, storage, distribution and refuelling for a sustainable transport sector: Hydrogen fuel cell vehicles. *Int J Hydrogen Energy* 52: 973–1004. https://doi.org/10.1016/j.ijhydene.2023.07.204
2. Foorginezhad S, Mohseni-Dargah M, Falahati Z, et al. (2021) Sensing advancement towards safety assessment of hydrogen fuel cell vehicles. *J Power Sources* 489: 229450. https://doi.org/10.1016/j.jpowsour.2021.229450
3. Ragul R, Shanmugasundaram N, Krishnakumar R (2022) PV system with zeta converter using anfis controller based gwo optimization. *In 2022 Int Conf Electron Renew Syst (ICEARS)*, 366–370. https://doi.org/10.1109/ICEARS53579.2022.9752008
4. Mohan A, Manitha PV (2023) Hybrid electric vehicles with V2X topology and smart energy management: An overview of their potential and limitations. *In 2023 2nd Int Conf Futur Technol (INCOFT)*, 1–8. https://doi.org/10.1109/INCOFT60753.2023.10449406
5. Sharma S, Deepa K, Sangeetha ST (2024) Study of electric vehicle charging prediction using different machine learning algorithms. *In 2024 10th Int Conf Adv Comput Commun Syst (ICACCS)*, 1050–1055. https://doi.org/10.1109/ICACCS60874.2024.10716983
6. Nair AHP, Sujith M (2022) Comparative path planning analysis for the recommended e-vehicle charging station. *In 2022 Int Conf Intell Innov Eng Technol (ICIIET)*, 238–244. https://doi.org/10.1109/ICIIET55458.2022.9967510
7. Jha A, Varshini CA, Poojitha Y, et al. (2024) EV battery health monitoring system. *In 2024 Int Conf Veh Technol Transp Syst (ICVTTS)*, 1–5. https://doi.org/10.1109/ICVTTS62812.2024.10763926
8. Mathi SC, Deepa K (2024) Soc estimation and comparative analysis of lithium polymer and lithium-ion batteries in unmanned aerial vehicles. *In 2024 First Int Conf Innov Commun Electr Comput Eng (ICICEC)*, 1–8. https://doi.org/10.1109/ICICEC62498.2024.10808488

9. Nyamathulla S, Dhanamjayulu C (2024) A review of battery energy storage systems and advanced battery management system for different applications: Challenges and recommendations. *J Energy Storage* 86: 111179. https://doi.org/10.1016/j.est.2024.111179
10. Boonraksa T, Boonraksa P, Pinthurat W, et al. (2024) Optimal battery charging schedule for a battery swapping station of an electric bus with a PV integration considering energy costs and peak-to-average ratio. *IEEE Access* 12: 36280–36295. https://doi.org/10.1109/ACCESS.2024.3374224
11. Dalai SK, Panda KP, Siwakoti YP, et al. (2024) Three-phase switched-capacitor boost self-balanced multilevel inverter for photovoltaic applications. *IEEE Trans Energy Convers* 39: 1818–1827. https://doi.org/10.1109/TEC.2024.3367733
12. Bhati N, Kalla UK (2024) Power factor corrected Y-cell modified boost converter fed battery charger for EV applications. *e-Prime Adv Electr Eng Electron Energy* 8: 100550. https://doi.org/10.1016/j.prime.2024.100550
13. Dadhaniya P, Maurya M, Vishwanath GM (2024) A bridgeless modified boost converter to improve power factor in EV battery charging applications. *IEEE J Emerg Sel Top Ind Electron* 5: 553–564. https://doi.org/10.1109/JESTIE.2024.3355887
14. Gaied H, Flah A, Kraiem H, et al. (2024) A comparison between the quality of two level and three levels bidirectional buck-boost converter using the neural network controller. *IEEE Access* 12: 94323–94336. https://doi.org/10.1109/ACCESS.2024.3403769
15. Mosaad MI, Salem F (2014) LFC based adaptive PID controller using ANN and ANFIS techniques. *J Electr Syst Inf Technol* 1: 212–222. https://doi.org/10.1016/j.jesit.2014.12.004
16. George MA, Kamat DV, Kurian CP (2024) Electric vehicle speed tracking control using an anfis-based fractional order PID controller. *J King Saud Univ-Eng Sci* 36: 256–264. https://doi.org/10.1016/j.jksues.2022.01.001
17. Aeggegn DB, Nyakoe GN, Wekesa C (2024) Anfis-controlled boost and bidirectional buck-boost DC-DC converters for solar PV, fuel cell, and bess-based microgrid application. *Int Trans Electr Energy Syst* 2024: 6484369. https://doi.org/10.1155/2024/6484369
18. Subramaniam U, Reddy KS, Kaliyaperumal D, et al. (2023) A mimo-anfis-controlled solar-fuel-cell-based switched capacitor z-source converter for an off-board EV charger. *Energies* 16: 1693. https://doi.org/10.3390/en16041693
19. Hsieh YC, Hsueh TC, Yen HC (2008) A dual-boost converter with zero voltage transition. *In 2008 IEEE Power Electronics Specialists Conference,* 692–696. https://doi.org/10.1109/PESC.2008.4592010
20. Kumar S, Niak MV (2024) Design and analysis of interleaved boost PFC converter for renewable energy system. *In 2024 IEEE Students Conference on Engineering and Systems (SCES)*, 1–6. https://doi.org/10.1109/SCES61914.2024.10652475
21. Rehman AU, Alblushi IGM, Khalid HM, et al. (2024) Techno economics and energy dynamics of a solar powered smart charging infrastructure for electric vehicles with advanced IoT based monitoring and RFID based security. *Sustainable Futures* 8: 100376. https://doi.org/10.1016/j.sftr.2024.100376
22. Shah N, Haque A, Mateen S, et al. (2024) Comparative analysis of control algorithms in isolated dual active bridge for ultra fast charging of electric vehicles. *In 2024 International Conference on Green Energy, Computing and Sustainable Technology (GECOST)*, 35–40. https://doi.org/10.1109/GECOST60902.2024.10474664

23. Singirikonda S, Obulesu YP, Kannan R, et al. (2022) Adaptive control-based isolated bidirectional converter for G2V & V2G charging with integration of the renewable energy source. *Energy Rep* 8: 11416–11428. https://doi.org/10.1016/j.egyr.2022.08.223
24. Balcı S, Kayabaşı A, Yıldız B (2021) Anfis based parameter estimating of a two-phase interleaved dual cascaded DC-DC boost converter for fuel cell supplied electric vehicles. *Balkan J Electr Comput Eng* 9: 410–416. https://doi.org/10.17694/bajece.856123
25. Babu TM, Chenchireddy K, Kumar KK, et al. (2024) Intelligent control strategies for grid-connected photovoltaic wind hybrid energy systems using ANFIS. *Int J Adv Appl Sci* 13: 497–506. http://doi.org/10.11591/ijaas.v13.i3.pp497-506
26. Mitrofanov SV, Kiryanova NG, Gorlova AM (2021) Stationary hybrid renewable energy systems for railway electrification: A review. *Energies* 14: 5946. https://doi.org/10.3390/en14185946
27. Rigogiannis N, Bogatsis I, Pechlivanis C, et al. (2023) Moving towards greener road transportation: A review. *Clean Technol* 5: 766–790. https://doi.org/10.3390/cleantechnol5020042
28. Ribeiro PJ, Dias G, Mendes JF (2024) Public transport decarbonization: An exploratory approach to bus electrification. *World Electr Veh J* 15: 81. https://doi.org/10.3390/wevj15030081
29. Aydogan H (2024) Electric vehicles and renewable energy. *J Phys Conf Ser* 2777: 012007. https://doi.org/10.1088/1742-6596/2777/1/012007
30. Guo L, Hu P, Wei H (2023) Development of supercapacitor hybrid electric vehicle. *J Energy Storage* 65: 107269. https://doi.org/10.1016/j.est.2023.107269

AIMS Press